ELSEVIER

Journal of Nuclear Materials 278 (2000) 242–250

journal of nuclear materials

www.elsevier.nl/locate/jnucmat

Nitrogen effect on precipitation and sensitization in cold-worked Type 316L(N) stainless steels

Yong Jun Oh *, Jun Hwa Hong

Department of Reactor Materials, Korea Atomic Energy Research Institute, P.O. Box 105, Yusong, Taejon 305-600, South Korea

Received 15 April 1999; accepted 24 September 1999

Abstract

The precipitation behavior and sensitization resistance of Type 316L(N) stainless steels containing different concentrations of nitrogen have been investigated at the aging condition of 700°C for cold work (CW) levels ranging from 0% (as solution annealed) to 40% reduction in thickness. The precipitation of $M_{23}C_6$ carbide and intermetallic compounds (χ, Laves and σ phase) was accelerated by increasing the CW level. Nitrogen in the deformed alloys retarded the inter- and intra-granular precipitation of the carbides at low and high CW levels respectively, whereas it increased the relative amount of the χ phase. Quantitative assessment of the degree of sensitization (DOS) using the double loop-electrochemical potentiokinetic reactivation (DL-EPR) tests indicated that CW levels up to 20% enhanced sensitization while 40% CW suppressed sensitization for all aging times. The increase in nitrogen content accelerated the sensitization at CW levels below 20%. This might be associated with the homogeneous distribution of dislocations and the lower tendency toward recrystallization exhibited in the alloys having higher nitrogen content.

PACS: 81.40.Ef; 81.65.Ku; 81.40.-z

1. Introduction

Austenitic stainless steels are the materials used for reactor internals and piping in light water reactor (LWR) and candidate materials for structural components in fast breeder reactors (FBR) because of their good corrosion resistance, weldability and high temperature mechanical properties. However, the steels undergo sensitization and become susceptible to intergranular corrosion (IGC) during thermal exposure at temperatures from 500°C to 850°C. The most generally accepted explanation of the sensitization is the chromium depletion model, proposed by Bain et al. [1], in which the sensitization is associated with the depletion of chromium adjacent to the grain boundaries as a consequence of the intergranular precipitation of $Cr_{23}C_6$ carbides. Decreasing the carbon content is therefore an effective method of improving the resistance to sensitization [2–5]. Since the degradation of mechanical properties by reduction in carbon content can be offset by the addition of nitrogen, the development of high IGC-resistant SSs has focused on alloys containing low carbon and an appropriate amount of nitrogen, designated 'LN grade' [6–11]. It has also been found that the nitrogen has a beneficial effect on the sensitization resistance [8–11]. Although the detailed kinetics have not been established yet, the retardation of sensitization has been confirmed for alloys with nitrogen additions of up to 0.16% [8].

Stainless steels are subjected to different levels of cold work (CW) during the final fabrication of components for numerous applications in nuclear industries. Many studies have been carried out to determine the relationship between cold work and the sensitization process. In a Type 304 SS, cold work dramatically

* Corresponding author. Tel.: +82-42 868 8561; fax: +82-42 868 8346.

E-mail address: yjoh@nanum.kaeri.re.kr (Y.J. Oh).

0022-3115/00/$ - see front matter
PII: S0022-3115(99)00255-X

accelerated sensitization and shifted the time–temperature–sensitization (TTS) curve to shorter times, the acceleration in Type 304 steel being attributed to the α′-martensite formed during deformation at ambient temperature [12–17]. It is well known that the kinetics of diffusion of chromium and carbon, which controls the chromium carbide formation, were much faster in the body-centered-cubic α′-martensite than in face-centered-cubic austenite [12,19–21]. On the other hand, the cold work effect in a Type 316 SS, in which the α′-martensite transformation does not occur during deformation at ambient temperature, has been explained in terms of the higher diffusivity of chromium and lower free energy barrier to carbide nucleation at grain boundaries in the deformed microstructure [16–18,22]. This is feasible because cold work produces extensive dislocation networks and grain boundary ledges which allow rapid pipe diffusion of the chromium and faster nucleation of carbides. Other possibilities for the sensitization acceleration with cold working can be related to the effects of point defects and microstructural sinks on diffusion reported by Mansur [23,24]. However, despite such possible mechanistic explanations, previous investigations on Type 316 SS have not included systematic empirical assessments.

The purpose of this work is to provide systematic data on the effect of nitrogen content on the microstructures and sensitization kinetics in the cold-worked steel. The observations are described in this paper to better understand the effects of deformation on the precipitation and sensitization in low carbon Type 316 SS having different levels of nitrogen.

2. Experimental procedure

2.1. Materials and specimen preparation

The chemical compositions of the Type 316L(N) SSs used in this investigation are given in Table 1; the nitrogen contents of the alloys ranged from 0.042 to 0.151 wt% at a fixed carbon level of about 0.020 wt%. All samples were initially solution annealed for 30 min at 1100°C, followed by water quenching. Some of the samples were then isothermally aged to evaluate the sensitization resistance in the undeformed condition. Other samples were cold-rolled at ambient temperature to reductions in thickness ranging from 5% to 40%, and then aged at 700°C for times up to 100 h.

2.2. Evaluation of the sensitization resistance

The susceptibility to sensitization of the alloys was determined using the double loop-electrochemical potentiokinetic reactivation (DL-EPR) test. Prior to this test, the oxalic acid test was used to screen the susceptibility to intergranular corrosion, according to the ASTM Standard A 262 Practice A. The DL-EPR test was performed by using a Gamry CMS105 DC Corrosion Measurement System at 30°C in a 0.5 M H_2SO_4 + 0.01 M KSCN solution deaerated with high purity nitrogen. The samples were polarized anodically from the corrosion potential to a potential of + 300 mV at a scan rate of 1.67 mV/s and then the potential was decreased at the same rate to the corrosion potential. The degree of sensitization (DOS) was measured by the ratio of maximum currents of reactivation loop (I_r) to anodic loop (I_a) [25,26].

2.3. Microstructural examination

The etched surfaces and the distribution of precipitates were examined using optical microscopy (OM) and scanning electron microscopy (SEM).

Specimens for transmission electron microscopy (TEM) were cut from the tested samples, mechanically polished and punched into 3 mm discs. Final thinning was performed by twin-jet polishing in a solution of perchloric acid:acetic acid:ethanol = 1:4:1, at 30 V and 5°C. Bulk extraction of the precipitates for X-ray diffraction analysis was carried out electrolytically in a 10% HCl in methanol electrolyte. The extracted residue was separated from the electrolyte using a centrifuge. The weight fraction of the precipitates was determined by weighing the bulk sample before and after partial dissolution and also weighing the extracted and dried residue. After weighing, the powder samples were mounted on a silicon single-crystal substrate, so that reduced

Table 1
Chemical compositions of the Type 316L(N) stainless steels investigated (in wt%)

Alloy	C	Mn	P	S	Si	Ni	Cr	Mo	Cu	N
L-1	0.018	0.95	0.006	0.002	0.67	12.21	17.78	2.36	0.20	0.042
L-2	0.019	0.97	0.007	0.002	0.70	12.46	17.23	2.38	0.21	0.103
L-3	0.023	0.96	0.007	0.002	0.67	12.19	17.18	2.41	0.21	0.151

Fe: bal.

background radiation and improved peak-to-background ratios were obtained. A Ricaku D/MAX-RC diffractometer fitted with a thin film measurement attachment was used to carry out the X-ray diffraction analysis. Cu Kα radiation was used.

In order to investigate the occurrence of α′-martensite in the alloys, the cold-worked samples were analyzed using a ferritescope and X-ray diffraction. Before analysis, the surfaces of samples were carefully polished with SiC paper, and then electrolytically polished in a solution of perchloric acid:acetic acid:ethanol = 1:4:1.

3. Results and discussion

3.1. Microstructural characteristics

3.1.1. Deformation effects on the precipitation

The microstructures of Type 316L(N) SS at various CW levels are presented in Fig. 1. The 0% and 5% cold-worked samples showed precipitates at grain and twin boundaries, identified as primarily $M_{23}C_6$ from X-ray diffraction and XEDS analysis. The 20% and 40% CW samples, on the other hand, exhibited precipitates at

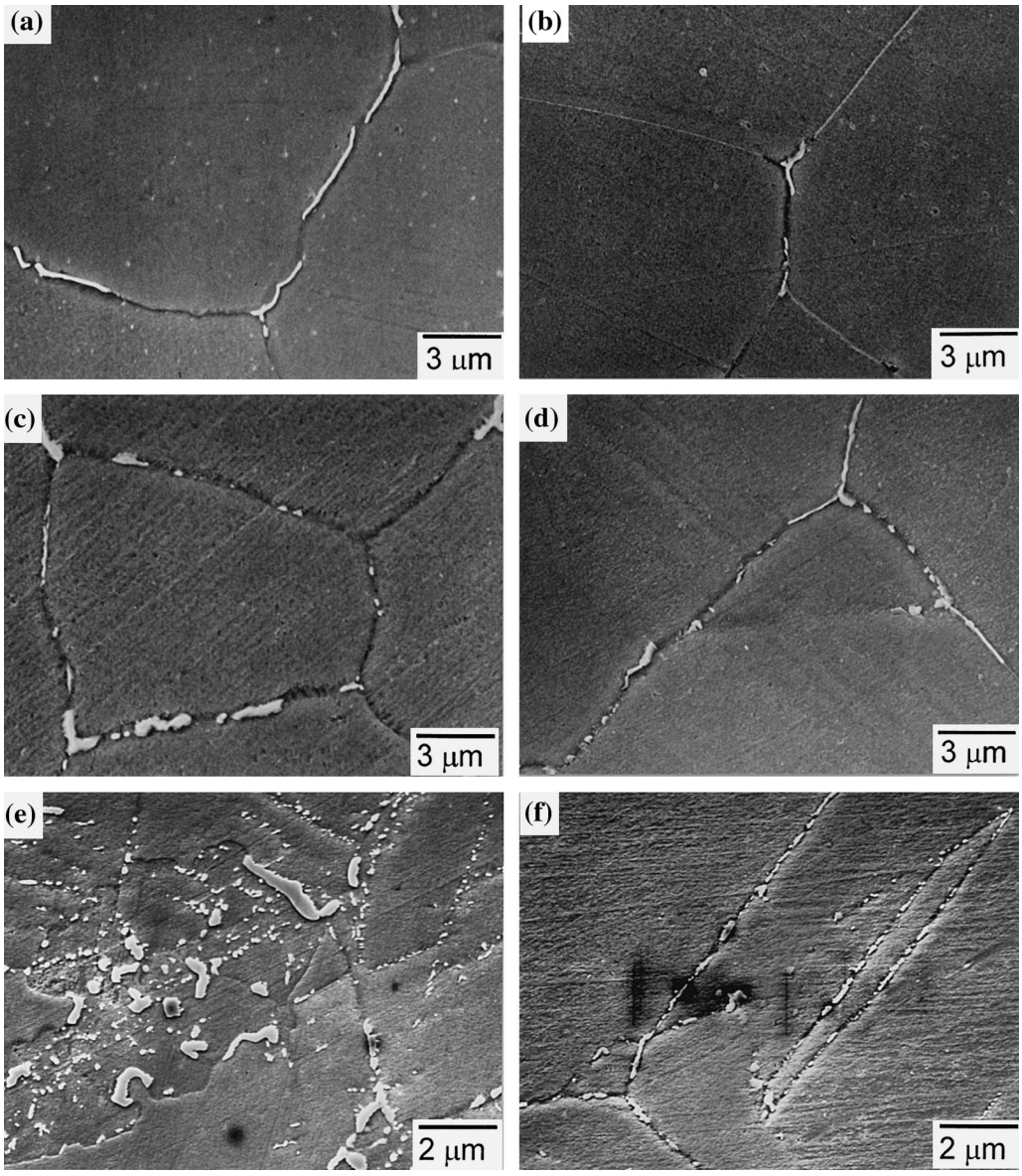

Fig. 1. SEM micrographs showing the precipitation in the L1 and L3 samples aged at 700°C for 30 h: (a) L1, 0% CW, (b) L3, 0% CW, (c) L1, 5% CW, (d) L3, 5% CW, (e) L1, 20% CW and (f) L3, 20% CW.

deformation bands as well as at grain and twin boundaries. The tendency for the intragranular precipitation increases with the decreasing nitrogen content in the alloys.

The quantitative analysis of the precipitates as a function of aging time at several prior CW levels is shown in Fig. 2. In the undeformed condition, the results indicate that the nitrogen retards precipitation at short aging times as shown in Fig. 2(a), which is consistent with the previous reports [8–11]. The enhancement of precipitation due to CW was small in the 5% CW samples, whereas it occurred noticeably in the 20% CW samples for the three alloys having different nitrogen contents. The retardation effect on precipitation by nitrogen is also valid in the cold-worked samples, showing larger amount of precipitates in the L1 alloy having lower nitrogen content.

The respective phases in the extracted mixture of the precipitates are identified using X-ray diffraction patterns. Fig. 3 shows X-ray diffraction lines on the precipitates extracted from the three alloys. For all samples, $M_{23}C_6$ was the main precipitate phase to form. The occurrence of the χ phase is not evident in the L1 alloy, whereas they are clearly identified in the L2 and L3 alloys having higher levels of nitrogen, as shown in Figs. 3(b) and (c). The figures also show that the occurrence of χ phase was accelerated by CW, but the amount of this phase relative to the carbide was not noticeably changed by CW. The presence of Laves phase was not clearly identified from X-ray diffraction because the peaks for the Laves phase were overlapped by prevalent peaks for carbide and sigma (σ) phase. But, from TEM observation and TEM-XEDS analysis, small Laves phase particles were found at grain boundaries for

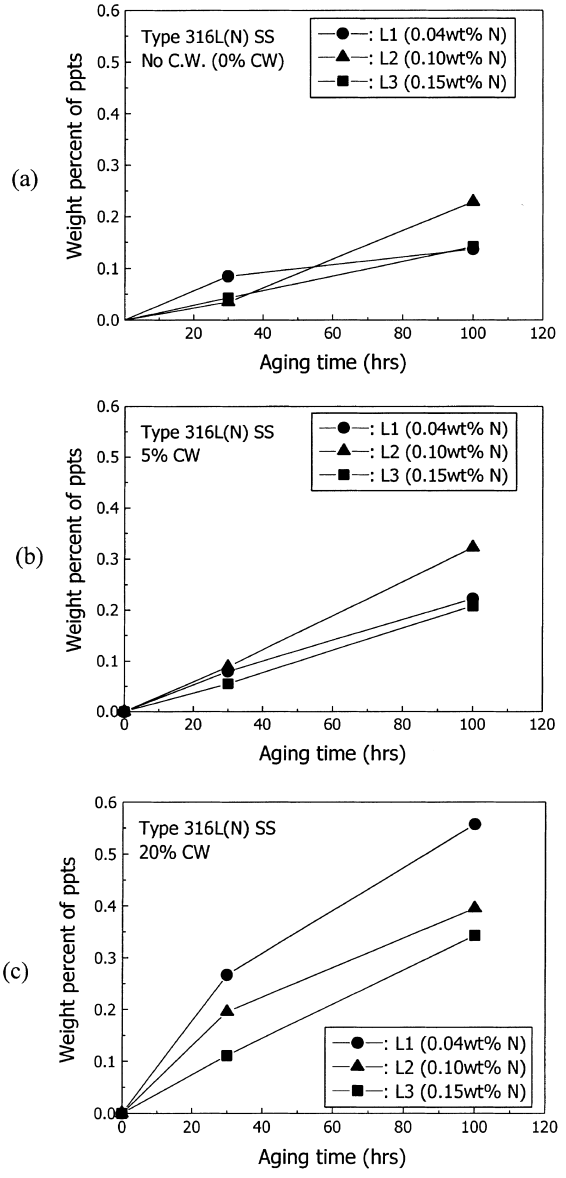

Fig. 2. Amount of bulk extracted residue as a function of aging time at three different cold work levels.

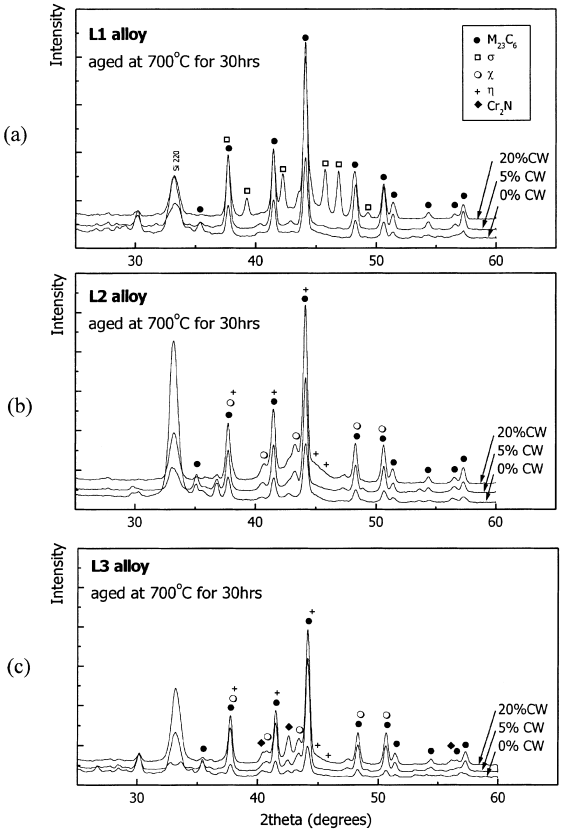

Fig. 3. X-ray diffraction spectra for the precipitates in the undeformed and deformed samples aged at 700°C for 30 h.

all samples with the same shape and chemical composition as the previous reports [11,27]. σ phase was only found in the 20% CW sample of the L1 alloy. The considerable enhancement of precipitation in the L1 alloy, as shown in Fig. 2(c), is partly associated with the occurrence of σ phase in this condition. Further details on the σ formation are dealt with in the following section in view of the deformed microstructure and recrystallization.

Cr_2N nitrides were identified in the cold-worked condition of the L3 alloy having 0.15 wt% nitrogen, while they were not evident in the undeformed condition. Their amounts were increased with an increasing degree of CW.

3.1.2. Deformed microstructures and recrystallization behavior

Dislocation density increases considerably by introducing cold working. The increase in the nitrogen content in alloys promotes the tendency toward the planar slip of dislocations by suppressing cross-slip [28]. Figs. 4(a) and (b) show the dislocations in the as-rolled samples to a 5% reduction in thickness of the L1 and L3 alloys, respectively. The L3 alloy having 0.15 wt% nitrogen exhibits co-planar arrays of nearly parallel dislocations, while the L1 alloy having 0.04 wt% nitrogen develops relatively tangled dislocation structures and some thick slip bands.

The strain-induced α' martensites were not found even in the 40% CW samples of the three alloys, although some shear band intersections, which are the potential nucleation sites for martensitic transformation, were found in the L1 alloy as shown in Fig. 4(c). The presence of ε martensites in the shear bands and stacking faults was not evident. The formation of the α' martensite in the cold-worked samples was not detected by the measurements of the magnetic permeability using a ferritescope nor by the analysis of the X-ray diffraction patterns, although the detailed results are not presented in this paper.

Figs. 5(a) and (b) show the dislocation microstructures after aging at 700°C for 30 h. The differences in the dislocation densities of the L1 and L3 alloys after the

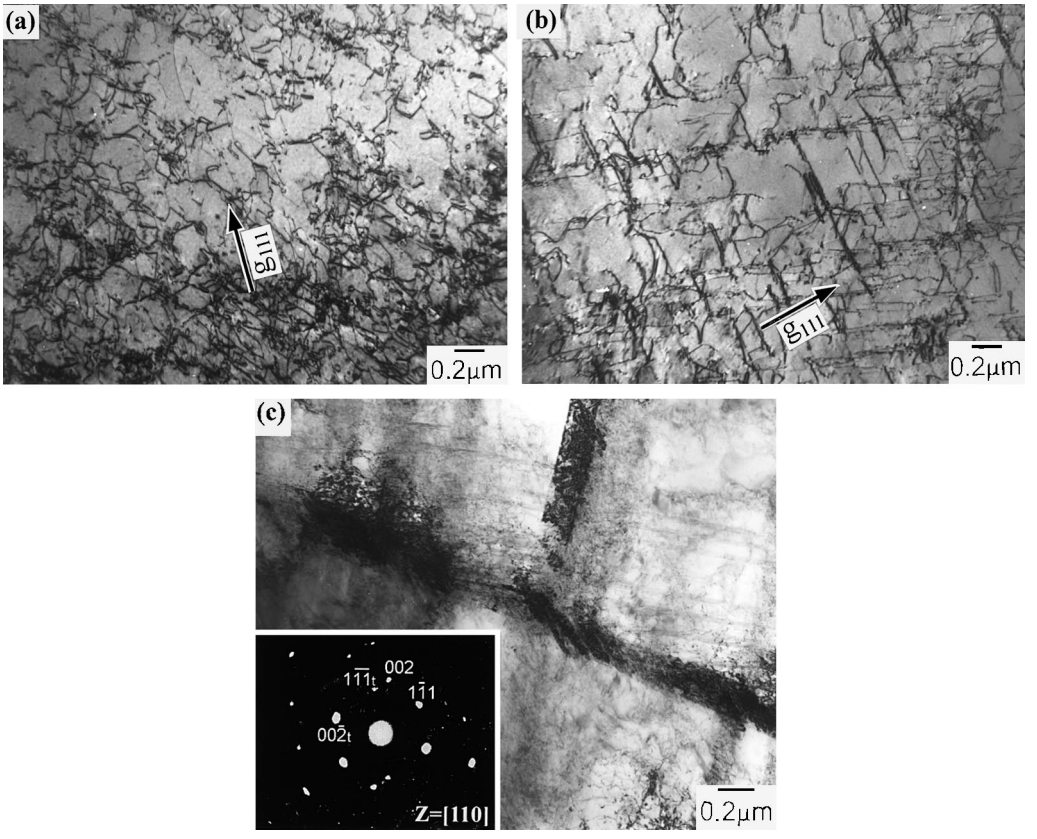

Fig. 4. Dislocation microstructures of the as-rolled materials. TEM micrographs of (a) and (b) show the slip characteristics in the 5% cold-worked condition of L1 and L3 alloys, respectively. (c) shows the deformation twin-fault region documenting absence of martensite in the 20% cold-worked L1 alloy. (The diffraction pattern on the bottom-left was taken from the junction of the twin-faults.)

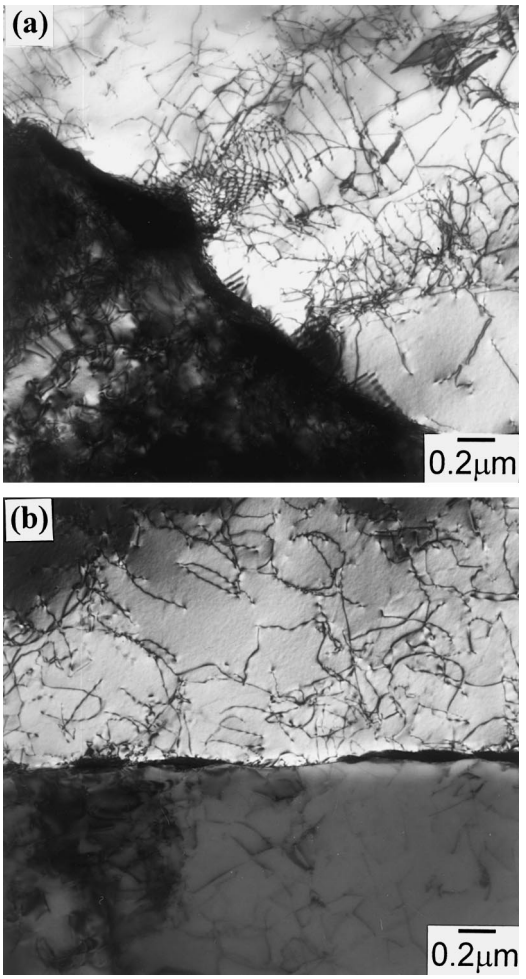

Fig. 5. Dislocation microstructures for the 5% cold-worked (a) L1 and (b) L3 samples after aging at 700°C for 30 h.

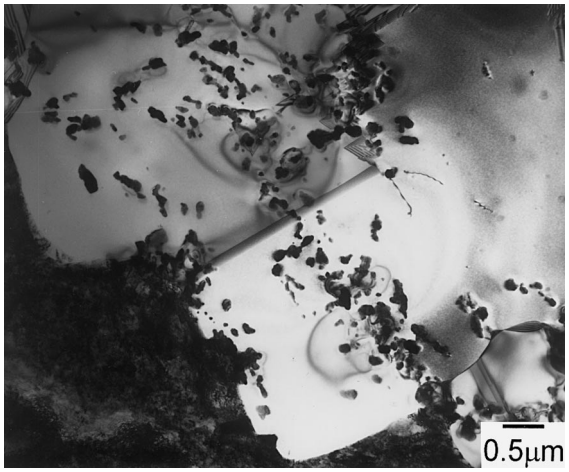

Fig. 6. TEM micrograph showing partial recrystallization in the L1 sample after 40% cold working and aging at 700°C for 30 h.

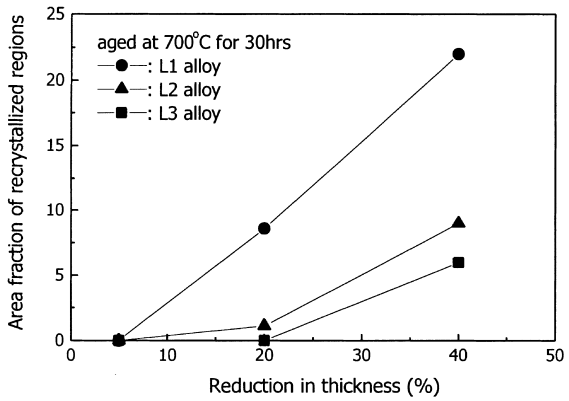

Fig. 7. The change of the recrystallized regions as a function of the reduction in thickness for the samples aged at 700°C for 30 h.

same aging times were not evidently distinguished. However, the homogeneity of the remaining dislocations near the grain boundaries was higher in the L3 than in the L1 alloy. The L1 alloy exhibited some released dislocation bands near the carbides at the grain boundaries, whereas the L3 alloy maintained a coplanar array of the dislocations.

The CW level above 20% induced partial recrystallization in the highly strained regions, as shown in Fig. 6. The quantitative measurement of the recrystallized areas, as shown in Fig. 7, indicates that nitrogen has an appreciable retarding effect on the partial recrystallization at 700°C. As already mentioned, nitrogen increases the homogeneity of the dislocations by inducing planar slip and suppresses the formation of highly tangled regions of dislocations and intensive slip bands in the matrix, which are the potential nucleation sites for recrystallization. These effects are also supported by the lower tendency toward intragranular precipitation in the L3 alloy than in the L1 alloy, as shown in Fig. 1.

The recrystallized regions contained a large number of precipitates (Fig. 6). Especially, the σ phase was only observed in the recrystallized regions and at the grain boundaries between the recrystallized and cold-worked grains. The nucleation of the σ phase requires high energy interfaces, particularly triple junctions of grain boundaries [29,30]. Spruiell et al. reported that the severely deformed and recrystallized regions could serve as effective sites for σ formation [31]. In this respect, our result on the formation of the σ phase in the deformed stainless steel was in good agreement with their observations.

3.2. Sensitization behavior

The quantitative results of the sensitization resistance from the DL-EPR test for the samples aged at 700°C are shown in Fig. 8. For the undeformed condition, the sensitization resistance at 700°C was highest in the L2 alloy with 0.11% nitrogen, but the enhancement of the sensitization by CW was most evident in the L3 and least in the L1 alloy. Healing or desensitization occurred in the 20% CW samples at long aging times, and the 40% CW specimens exhibited high sensitization resistance for all aging times. Fig. 9 represents the dependency of EPR-DOS on the degree of CW in the three alloys aged at 700°C for 30 h, the aging time at which the healing effect was not yet apparent. In the L2 and L3 alloys containing more than 0.10% nitrogen, the dependency on CW is noticeably high at 5% CW and decreases at the higher level of 40%. On the other hand, in the L1 alloy with low nitrogen content, the dependency is low and does not change up to 20% CW.

If the sensitized condition is defined as the level of more than 10% of EPR DOS from Fig. 8, the sensitized region can be depicted on the plot of aging time vs. degree of CW, as shown in Fig. 10. The locus of the line

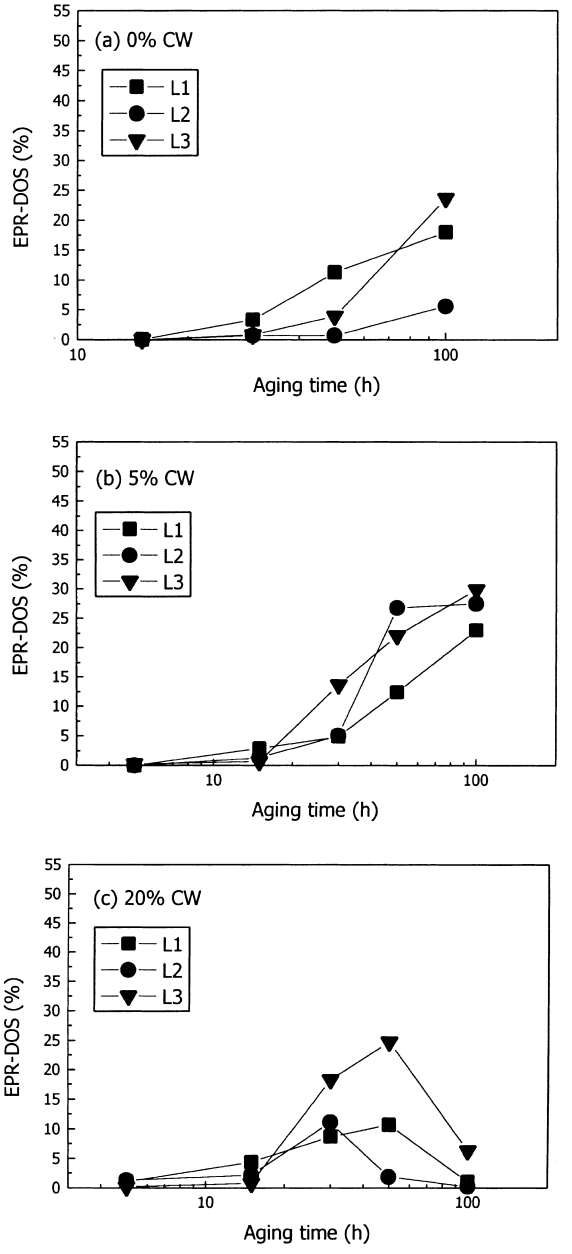

Fig. 8. The results of the DL-EPR test for undeformed and deformed samples aged at 700°C: (a) L1, (b) L2 and (c) L3 alloys.

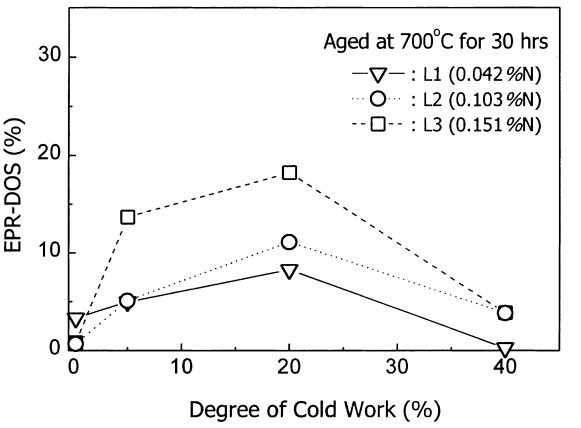

Fig. 9. The variation of EPR-DOS as a function of degree of cold work (%) in the alloys with different nitrogen contents after aging at 700°C for 30 h.

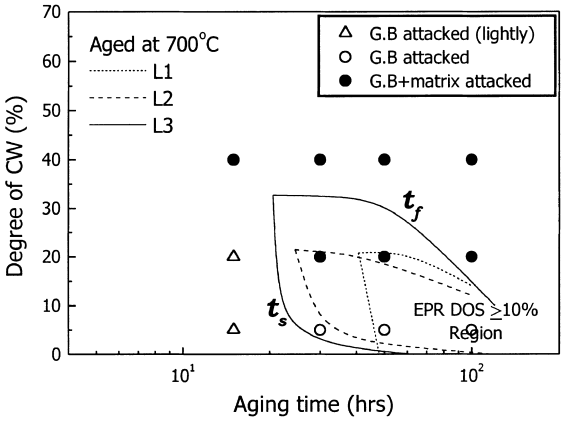

Fig. 10. Time-deformation-sensitization (TDS) diagrams for the alloys aged at 700°C. The lines were obtained from Fig. 9 by connecting the times for 10% EPR-DOS at different CW levels.

in the diagrams surrounds the region exhibiting more than 10% of EPR DOS. The constructed diagrams characterize the combination of appropriate CW and heat treatment times to avoid sensitization at 700°C in the alloys. In the diagrams shown in Fig. 10, the increase in nitrogen content shifted the time for sensitization (t_s) to a shorter time and expanded the sensitized region.

The results of the sensitization resistance in the undeformed condition are consistent with the precipitation behaviors shown in Fig. 2, showing that the alloy having larger amounts of precipitates exhibits faster sensitization. On the other hand, it is interesting that the results for the deformed samples do not show any proportional relationship between each other. The inverse is rather true. In the 20% CW samples, this can be explained by the differences in the intragranular precipitation and the recrystallization behaviors in the three alloys. As already mentioned, the alloys having lower nitrogen content exhibited enhanced recrystallization and intragranular precipitation. The continuous movement of the boundary due to the expansion of the recrystallized regions does not result in locally significant chromium depletion near the grain boundaries, despite the enhanced precipitation.

However, for the 5% CW samples exhibiting no apparent intragranular precipitation and partial recrystallization, the reason for the lower enhancement of the sensitization in the alloy having lower nitrogen content could not be explicitly explained. This is possibly attributed to the relatively high rate of lattice diffusion of the chromium to the carbides in the L1 alloy, reducing the relative contribution from the grain boundary diffusion at 700°C. As a whole, the carbides at the grain boundaries were thicker in the L1 alloy than in the L2 and L3 alloys. In particular, some carbides at the grain boundaries in the 5% CW L1 sample exhibited extruded surfaces into the adjacent grains whereas the carbides in the L2 and L3 alloys had a narrow, elongated, plate-like shape, as shown in Fig. 11 and Figs. 1(c) and (d). These observations might suggest that the growth of carbides in the L1 alloy was rapidly proceeded by the high lattice diffusion of the chromium, rather than the grain boundary diffusion. The locally intensive distribution of the dislocations in L1 alloy can further accelerate the diffusion directly to the grain boundary carbides, resulting in larger carbides, but with less severe Cr-depleted regions adjacent to the grain boundaries.

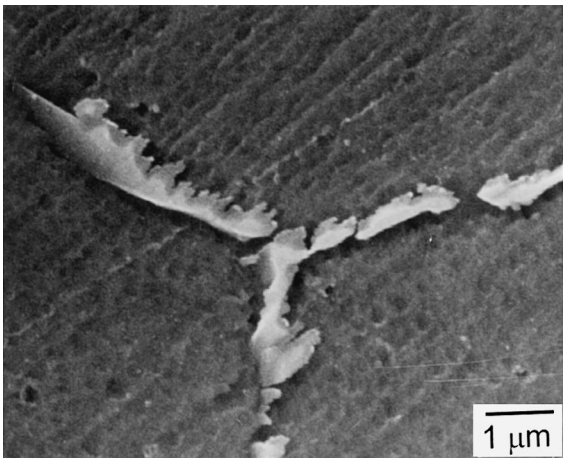

Fig. 11. The morphology of the carbides in the 5% CW L1 alloy aged at 700°C for 30 h supporting rapid lattice diffusion.

The formation of the Cr_2N phase in the deformed L3 alloys can also accelerate the sensitization. However, as shown in Fig. 2, the total amounts of precipitates at the same CW levels and aging times are lower in the L3 than in the L1 and L2 alloys, even excluding the intermetallic phases. Thus, considering that the contribution to the chromium depletion from the Cr_2N phase is lower than that from $M_{23}C_6$ carbides because nitrides contain a Cr-to-N ratio less than that of the $M_{23}C_6$ carbides [32], the formation of the Cr_2N phase is not believed to be an important factor in enhancing the sensitization in the deformed L3 alloy.

4. Conclusions

The precipitation behavior and sensitization resistance of Type 316L(N) stainless steels containing different concentrations of nitrogen have been investigated at the aging condition of 700°C for CW levels ranging from a 0% (as solution annealed) to 40% reduction in thickness. The following conclusions were drawn.

1. Cold work accelerated the precipitation of the carbides ($M_{23}C_6$) and intermetallic compounds (χ, Laves and σ phases). The nitrogen retarded the inter- and intragranular precipitation of the carbides at low and high CW levels, respectively. However, the relative amounts of the χ phase somewhat increased by increasing the nitrogen content. Deformation induced the formation of Cr_2N phase in the L3 alloy having 0.15 wt% N.
2. The tendency toward recrystallization of the deformed matrix increased by decreasing the nitrogen content in the alloy. The nitrogen induced the homogeneous distribution of the dislocations and suppressed the development of the locally intensive slip bands during cold working, which reduce the nucleation sites for recrystallization.
3. The DL-EPR test results indicated that CW levels up to 20% enhanced sensitization while 40% CW suppressed sensitization at all aging times. The increase in the nitrogen content at the similar carbon content accelerated the sensitization at CW levels below 20%.
4. The increased dislocation density was the main cause for the accelerated sensitization in the deformed al-

loys. The higher enhancement of the sensitization in the alloys having higher nitrogen content might be associated with the homogeneous distribution of the dislocations and the lower tendency toward partial recrystallization.

Acknowledgements

This work has been carried out as a part of the Reactor Pressure Boundary Materials Project under the Nuclear R&D Program by MOST in Korea. The authors acknowledge the experimental assistance of Mr M. H. Suh from Chungnam National University and Dr M. C. Kim with KAERI.

References

[1] E.C. Bain, R.H. Aborn, J.J.B. Rutherford, Trans. Am. Soc. Steel Treating 21 (1933) 481.
[2] C.L. Briant, R.A. Mulford, E.L. Hall, Corrosion 38 (1982) 468.
[3] S.M. Bruemmer, Corrosion 42 (1986) 29.
[4] R. Pascali, A. Benvenuti, D. Wenger, Corrosion 40 (1984) 21.
[5] H.S. Betrabet, K. Nishimoto, B.E. Wilde, W.A.T. Clark, Corrosion 43 (1987) 77.
[6] P.R. Levey, A. van Bennekom, Corrosion 51 (1995) 911.
[7] J-O. Nilsson, T. Thorvaldsson, Scand. J. Metall. 15 (1985) 83.
[8] T.A. Mozhi, W.H.S. Betrabet, V. Jagannathan, B.E. Wilde, W.A.T. Clark, Scripta Metall. 20 (1986) 723.
[9] C.L. Briant, Scripta Metall. 21 (1987) 71.
[10] S. Danyluk, J.-Y. Park, Scripta Metall. 16 (1982) 769.
[11] Y.J. Oh, W.S. Ryu, C. Sung, I.H. Kuk, J.H. Hong, J. Mater. Res. 14 (1999) 390.
[12] C.L. Briant, A.M. Ritter, Metall. Trans. 11A (1980) 2009.
[13] E.A. Trillo, R. Beltran, J.G. Maldonado, R. Romero, L.E. Murr, W.W. Fisher, H. Advani, Mater. Char. 35 (1995) 99.
[14] A.H. Advani, L.E. Murr, D.J. Matlock, R.J. Romero, W.W. Fisher, P.M. Tarin, J.G. Maldonado, C.M. Cedillo, R.L. Miller, E.A. Trillo, Acta Metall. Mater. 41 (1993) 2589.
[15] E.P. Butler, M.G. Burke, Acta Metall. 34 (1986) 557.
[16] Vijay Shrinivas, S.K. Varma, L.E. Murr, Metall. Trans. 26A (1994) 661.
[17] N. Parvathavarthini, R.K. Dayal, S.K. Seshadri, J.B. Gnanamoorthy, J. Nucl. Mater. 168 (1989) 83.
[18] S.K. Mannan, R.K. Dayal, M. Vijayalakshmi, N. Parvathavarthini, J. Nucl. Mater. 126 (1984) 1.
[19] A.H. Advani, L.E. Murr, D.G. Atteridge, R. Chelakara, Metall. Trans. 22A (1991) 2917.
[20] C.L. Briant, A.M. Ritter, Metall. Trans. 11A (1980) 2009.
[21] C.J. Smithels, Metals Reference Book, Butterworths, Boston, 1976, p. 874.
[22] C.L. Briant, Effect of nitrogen and cold work on the sensitization of austenitic stainless steels, Electric Power Research Institute Report EPRI-NP-2457, 1982.
[23] L.E. Murr, A. Advani, S. Shankar, D.G. Atteridge, Mater. Char. 24 (1990) 135.
[24] L.K. Mansur, J. Nucl. Mater. 83 (1979) 109.
[25] L.K. Mansur, A.D. Brailsford, W.G. Wolfer, J. Nucl. Mater. 105 (1982) 36.
[26] R. Katsura, M. Kodama, Nishimura, Corrosion 48 (1992) 384.
[27] A.P. Majidi, M.A. Streicher, Corrosion 40 (1984) 585.
[28] P.J. Maziasz, Proc. MiCon '86: Optimization of Processing, Properties and Service Performance Through Microstructural Control, ASTM STP 979, Am. Soc. for Testing and Materials, Philadelphia, PA, 1988, p. 116.
[29] R.E. Stoltz, J.B. Vander Sande, Metall. Trans. 11A (1980) 1033.
[30] B. Weiss, R. Stickler, Metall. Trans. 3A (1972) 851.
[31] P.J. Maziasz, J. Nucl. Mater. 85&86 (1979) 713.
[32] J.E. Spruiell, J.A. Scott, C.S. Ary, R.L. Hardin, Metall. Trans. 4A (1973) 1533.